Electro-osmotic and pressure-driven flow of viscoelastic fluids in microchannels: Analytical and semi-analytical solutions

L. L. Ferrás, A. M. Afonso, M. A. Alves, J. M. Nóbrega, and F. T. Pinho

Citation: Physics of Fluids **28**, 093102 (2016); doi: 10.1063/1.4962357
View online: http://dx.doi.org/10.1063/1.4962357
View Table of Contents: http://scitation.aip.org/content/aip/journal/pof2/28/9?ver=pdfcov
Published by the AIP Publishing

Electro-osmotic and pressure-driven flow of viscoelastic fluids in microchannels: Analytical and semi-analytical solutions

L. L. Ferrás,[1,a)] A. M. Afonso,[2,b)] M. A. Alves,[2,c)] J. M. Nóbrega,[1,d)] and F. T. Pinho[3,e)]

[1]*Institute for Polymers and Composites/I3N, University of Minho, Campus de Azurém, 4800-058 Guimarães, Portugal*

[2]*Departamento de Engenharia Química, Centro de Estudos de Fenómenos de Transporte, Faculdade de Engenharia da Universidade do Porto, Rua Dr. Roberto Frias s/n, 4200-465 Porto, Portugal*

[3]*Departamento de Engenharia Mecânica, Centro de Estudos de Fenómenos de Transporte, Faculdade de Engenharia da Universidade do Porto, Rua Dr. Roberto Frias s/n, 4200-465 Porto, Portugal*

(Received 29 March 2016; accepted 18 August 2016; published online 29 September 2016)

In this work, we present a series of solutions for combined electro-osmotic and pressure-driven flows of viscoelastic fluids in microchannels. The solutions are semi-analytical, a feature made possible by the use of the Debye–Hückel approximation for the electrokinetic fields, thus restricted to cases with small electric double-layers, in which the distance between the microfluidic device walls is at least one order of magnitude larger than the electric double-layer thickness. To describe the complex fluid rheology, several viscoelastic differential constitutive models were used, namely, the simplified Phan-Thien–Tanner model with linear, quadratic or exponential kernel for the stress coefficient function, the Johnson-Segalman model, and the Giesekus model. The results obtained illustrate the effects of the Weissenberg number, the Johnson-Segalman slip parameter, the Giesekus mobility parameter, and the relative strengths of the electro-osmotic and pressure gradient-driven forcings on the dynamics of these viscoelastic flows. *Published by AIP Publishing.* [http://dx.doi.org/10.1063/1.4962357]

NOMENCLATURE

Symbols	Definition
a	Non-affine slip parameter
C	Ion concentration
$\mathbf{D}$	Rate of deformation tensor
$\mathbf{E}$	External electric field
e	Elementary charge
erf $(\cdot)$	Error function
$E_x \equiv -\mathrm{d}\phi/\mathrm{d}x$	Constant streamwise gradient of electric potential generated by electrodes
$f\,(tr\boldsymbol{\tau})$	Scalar function of the trace of the polymer extra stress tensor
H	Half-channel width/thickness
k_B	Boltzmann constant
N_A	Avogadro's number

a)Electronic mail: luis.ferras@dep.uminho.pt
b)Electronic mail: aafonso@fe.up.pt
c)Electronic mail: mmalves@fe.up.pt
d)Electronic mail: mnobrega@dep.uminho.pt
e)Electronic mail: fpinho@fe.up.pt

n_o	Ion density
$p_{,x}$	Streamwise pressure gradient
p	Pressure
$\bar{Q}$	Dimensionless flow rate
t	Time
T	Absolute temperature
$\mathbf{u}$	Velocity vector
u	Streamwise velocity component
u_{sh}	Helmholtz-Smoluchowski electro-osmotic velocity
U	Mean velocity
Wi	Weissenberg number for the pure pressure driven case
Wi_κ	Weissenberg number
x	Streamwise coordinate
y	Transverse coordinate
z	Valence of the ions
$\bar{\cdot}$	The overline represents a dimensionless quantity

Greek Symbols	Definition
α	Mobility parameter
Γ	Ratio of pressure to electro-osmotic driving forcings
ε	Parameter of the Phan-Thien–Tanner model
ϵ	Electrical permittivity of the solution
ζ	Wall zeta potential
η	Polymer viscosity coefficient
κ^2	Debye–Hückel parameter
λ	Relaxation time of the fluid
ξ	Electric double layer thickness
ρ	Fluid density
ρ_e	Net electric charge density
$\boldsymbol{\tau}$	Polymeric extra-stress tensor
τ_{xy}	Shear stress
τ_{xx}	Normal stress
τ_{yy}	Normal stress
Φ	Electric potential
ϕ	Electric potential in the streamwise direction (imposed)
ψ	Potential field in the transverse direction (induced)

I. INTRODUCTION

Electro-osmosis[1] is currently a rich research topic due to its applicability in micro- and nano-devices with applications in medicine, biochemistry, and several other industrial processes, but the idea of creating motion using an external electric field goes back two centuries ago, when Reuss[2] investigated this phenomenon experimentally, using a porous clay. Experimental, theoretical, and numerical efforts for the understanding of such physical phenomenon have intensified in recent years, with several research groups contributing actively to the subject. A large number of applications in microfluidics use biofluids, which are usually complex in their structure requiring equally complex constitutive equations to describe their rheology and the ensuing flows. In particular, viscoelastic fluids usually exhibit normal stress differences, shear-thinning viscosity, and memory effects and their rheological behavior can be described by differential viscoelastic equations, which are related or are contained in the Phan-Thien—Tanner (PTT)[3,4] and Giesekus[6] models, as in the case of blood,[7,8] synovial fluid,[9] or other biofluids possessing long chain molecules. Therefore, analytical solutions are useful not just to describe the phenomena at hand but also to improve our understanding about them.

For Newtonian fluids, Burgreen and Nakache[10] presented an analytical study of electrokinetic flow inside very fine capillary channels of rectangular cross section, extending previous studies that were restricted to channels of large electrokinetic radius (the electrokinetic effects are confined to the area close to the capillary wall) or to interfaces with low surface potentials, whereas Rice and Whitehead[11] presented the corresponding flow solution for a cylindrical geometry. Arulanandam and Li[12] investigated numerically the electro-osmotic flow (EOF) in rectangular microchannels by solving the 2D Poisson-Boltzmann and momentum equations, whereas Dutta and Beskok[13] studied analytically the 2D mixed electro-osmotic/pressure-driven flow. For non-Newtonian inelastic fluids described by the Ostwald–de Waele Power-Law model, Das and Chakraborty[14] presented analytical solutions that describe the transport characteristics in channel flow and Berli and Olivares[15] introduced a theoretical description of electro-osmotic flow through slits and cylindrical microchannels using also the Power-Law model, and also the Bingham and Eyring models. Zhao and Yang[16] investigated theoretically the electro-osmotic mobility of Power-Law fluids in channel flows, which was later generalized for the Carreau model.[17] Hence, the description of these simple flows for generalized Newtonian fluids is essentially complete.

For non-Newtonian viscoelastic fluids, the existing analytical solutions are more recent because of their associated complexity. Afonso *et al.*[18,19] provided analytical solutions of mixed electro-osmotic/pressure-driven flows of viscoelastic fluids in microchannels, including the case of electro-osmotic flow under asymmetric zeta potentials at both walls. Earlier, Park and Lee[20] extended the theory of the Newtonian Helmholtz-Smoluchowski velocity to incorporate the viscoelastic behavior described by the simplified Phan-Thien—Tanner model (sPTT) in rectangular channels. Sousa *et al.*[21] extended the analysis of Afonso *et al.*[18,19] by considering the formation of a skimming layer without polymer additives near the walls, and Dhinakaran *et al.*[22] analyzed the channel flow for the full PTT model with non-zero second normal-stress difference by considering the full Gordon-Schowalter convected derivative but restricting the analysis to pure electro-osmosis flow (without a pressure gradient). Recently, Afonso *et al.*[23] presented analytical solutions for fully developed EOF by considering polymer solutions described by the sPTT and FENE-P[24] models with a Newtonian solvent. Hayat *et al.*[25] presented an exact solution for the electro-osmotic flow of a generalized Burgers fluid and more recently Afonso *et al.*[26] also solved analytically the channel flow of stratified immiscible fluids driven by electro-osmosis assuming a planar interface between the two viscoelastic immiscible fluids, an arrangement usually employed for fluid pumping using electrokinetic effects.

In this work, analytical solutions are presented for electro-osmotic and pressure-driven fully developed channel flows of viscoelastic fluids modeled by the quadratic and exponential PTT model,[3,4] the Johnson-Segalman[27] model, and the Giesekus[6] model. For the quadratic PTT model, the solution is applicable for simultaneous electro-osmotic and pressure driven flows, while for the remaining viscoelastic models the analytical solution is only given for the pure electro-osmotic flow. The derived solutions complete the set of possible cases, as summarized in Table I, and allow a better understanding of the viscoelastic flow behavior in the presence of an electric field. In this paper, we extend previous works to more complex and realistic viscoelastic models,

TABLE I. Analytical (A) and semi-analytical (SA) solutions for the sPTT, PTT, Johnson-Segalman and Giesekus models. Only the solutions tagged with "This work (A)" are presented in this work.

	Pure EO	EO and PD	Pure PD
Linear sPTT	Afonso *et al.*[18] (A)	Afonso *et al.*[18] (A)	Oliveira and Pinho[30] (A)
Quadratic sPTT	This work (A)	This work (A)	This work (A)
Exp. sPTT	This work (A)	(SA)	Oliveira and Pinho[30] (A)
Linear PTT	Dhinakaran *et al.*[22] (A)	(SA)	Alves *et al.*[31] (A)
Exp. PTT	(SA)	(SA)	(SA)
Johnson-Segalman	Dhinakaran *et al.*[22] (A)	(SA)	Alves *et al.*[31] (A)
Giesekus	This work (A)	(SA)	Yoo and Choi[33] (A)

and these theoretical studies can also be useful to computational rheology, either for verification purposes of their numerical methods or to define fully developed inlet boundary conditions.

The remainder of this paper starts with the formulation of the problem and the set of governing equations, including the nonlinear Poisson–Boltzmann equation that governs the electric double layer field and the added body force to the momentum equation, caused by the applied electrical field. We then arrive at the basic set of equations for all the analytical solutions, and afterwards each viscoelastic model is analyzed in detail and the simplifications required to obtain the analytical solutions are presented. A discussion of the effects of the various relevant dimensionless parameters upon the flow characteristics is presented before the Conclusions of the work.

II. PROBLEM FORMULATION AND GOVERNING EQUATIONS

Consider the combined electro-osmotic and pressure-driven flow of a viscoelastic fluid between two parallel plates. The flow geometry and coordinate system are shown in Fig. 1. The streamwise coordinate and velocity component are x and u, respectively, the transverse coordinate is y and there is no flow or gradients in the spanwise direction z, which is assumed to be much larger than H ($2H$ is the channel width). The flow direction in the conditions illustrated in Fig. 1 is from left to right, but the solutions described here remain valid for the corresponding opposed flow conditions. The migration of ions naturally arises due to the interaction between the dielectric walls and the polar fluid. Here, the two negatively charged walls of the microchannel attract counter-ions forming layers of positively charged fluid near the walls and repel the co-ions. Very thin layers of immobile counter-ions cover the walls, known as the Stern layers, followed by thicker more diffuse layers of mobile counter-ions, the two layers near the wall forming what is called the Electrical Double Layer (EDL). The global charge of the flow domain remains neutral, but since the two EDLs are very thin the core is essentially neutral. Applying a DC potential difference between the two electrodes at the inlet and outlet generates an external electric field that exerts a body force on the ions of the EDL, which move along the channel dragging the neutral liquid core. The pressure difference that can also be applied between the inlet and outlet can act in the same direction of the electric field or in the opposite direction. Due to the symmetry of the geometry, only half of the channel ($0 \leq y \leq H$) is considered in the analysis. At the wall, the no-slip condition applies; whereas on the centreplane, $y = 0$, the symmetry condition was used. Since the flow is fully developed, the velocity and stress fields only depend on the transverse coordinate y.

The steady, fully developed flow of the incompressible viscoelastic fluid is governed by the continuity,

$$\nabla \cdot \mathbf{u} = 0 \tag{1}$$

and the momentum equation,

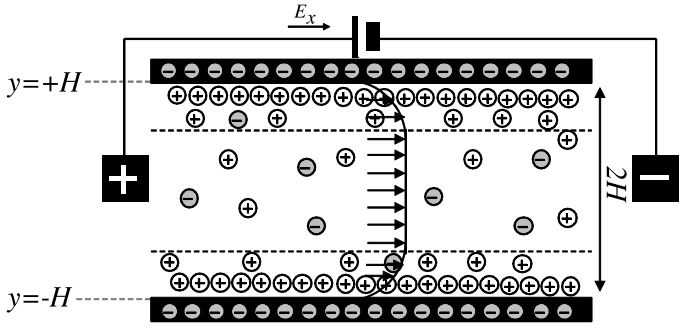

FIG. 1. Schematic of the flow in a planar microchannel.

$$\rho\frac{\mathrm{D}\mathbf{u}}{\mathrm{D}t} = \nabla\cdot\boldsymbol{\tau} - \nabla p + \rho_e\mathbf{E}, \tag{2}$$

where $\mathbf{u}$ is the velocity vector, p the pressure, ρ the fluid density, $\boldsymbol{\tau}$ the fluid extra-stress tensor, $\mathbf{E}$ the electric field, and ρ_e is the net electric charge density in the fluid.

A. Constitutive equations

In order to obtain a closed system of equations, a constitutive equation for the polymeric extra-stress tensor, $\boldsymbol{\tau}$, must be employed. Several constitutive relations for viscoelastic fluids have been proposed in the literature.[3,4,6,24,27] The development of efficient, more realistic models is still a fertile ground in rheology,[28] and so far no model is generally exact, since the adequate choice of the constitutive equation for a particular application depends on both the physical characteristics of the working fluid and type of flow. Therefore, the ideal scenario where for each fluid there is a model describing correctly its fluid rheological and flow properties has not yet been fully achieved. For instance, models presenting constant shear viscosity, such as the Upper-Convected Maxwell (UCM) model, Oldroyd-B, or FENE-CR[29] models, should not be used when the viscosity of the real fluid varies with the shear rate, as with shear-thickening or shear-thinning fluids. Such types of fluid should instead be described by the PTT,[3,4] Giesekus[6] or FENE-P[24] models in their original or modified forms,[5] amongst others. Therefore, and as stated before, in this work we adopted three constitutive equations that are capable to represent well a large number of biofluids used in microfluidic applications.[7–9] Those various rheological equations of state can be written in a compact form as the following generic equation:

$$f\left(tr\boldsymbol{\tau}\right)\boldsymbol{\tau} + \lambda\left(\frac{\partial\boldsymbol{\tau}}{\partial t} + \mathbf{u}\cdot\nabla\boldsymbol{\tau} - \left[\left(\nabla\mathbf{u}\right)^T\cdot\boldsymbol{\tau} + \boldsymbol{\tau}\cdot\nabla\mathbf{u}\right] + \left(1-a\right)\left(\mathbf{D}\cdot\boldsymbol{\tau} + \boldsymbol{\tau}\cdot\mathbf{D}\right)\right) + \alpha\frac{\lambda}{\eta}\boldsymbol{\tau}\cdot\boldsymbol{\tau} = 2\eta\mathbf{D}, \tag{3}$$

where $\mathbf{D} = \left(\nabla\mathbf{u} + \nabla\mathbf{u}^T\right)/2$ is the rate of deformation tensor, λ the relaxation time of the fluid, η the polymer viscosity coefficient, $f\left(tr\boldsymbol{\tau}\right)$ is a scalar function of the trace of the polymer extra-stress tensor, a is the non-affine slip parameter, and α is the mobility parameter.

Eq. (3) allows the choice of a specific constitutive model by an appropriate selection of parameters α, ε, and a. For instance, the simplified Phan-Thien and Tanner (sPTT) model,[3,4] derived on the basis of network theory arguments, can be obtained assuming $\alpha = 0$, $a = 1$ and the stress coefficient function, $f\left(tr\boldsymbol{\tau}\right)$, can take any of the following forms:

$$f(\tau_{kk}) = \begin{cases} 1 + \dfrac{\varepsilon\lambda}{\eta}\tau_{kk} & \text{linear PTT} \\ 1 + \dfrac{\varepsilon\lambda}{\eta}\tau_{kk} + \dfrac{1}{2}\left(\dfrac{\varepsilon\lambda}{\eta}\tau_{kk}\right)^2 & \text{quadratic PTT} \\ \exp\left(\dfrac{\varepsilon\lambda}{\eta}\tau_{kk}\right) & \text{exponential PTT} \end{cases} \tag{4}$$

with ε being an extensibility parameter of the model which limits the fluid extensional viscosity. Note that Einstein's convention of summation over repeated indices is used in Eq. (4). The sPTT model presents shear-thinning viscosity and a zero second normal-stress difference coefficient.

The full PTT model is obtained by setting $a \neq 1$ and the same scalar stress functions of Eq. (4). In this model, the slip parameter, a, takes into account the non-affine motion between the polymer molecules and the continuum.

The Giesekus model[6] is recovered when $\alpha \neq 0$, $\varepsilon = 0$, and $a = 1$. This model was derived on the basis of the kinetic theory for packed polymer chains, as for the full PTT model, and it also exhibits a non-zero second normal-stress difference in steady shear flows. Finally, the Johnson-Segalman constitutive equation,[27] used to describe some dilute polymer solutions, is obtained when $\alpha = 0$, $\varepsilon = 0$, and $a \neq 1$. Eq. (3) reverts to the UCM model when $\alpha = 0$, $\varepsilon = 0$, and $a = 1$.

B. Electric potential

The electrostatic field is related to the electric potential, Φ, by $\mathbf{E} = -\nabla\Phi$ and Φ is governed by $\nabla^2\Phi = -\frac{\rho_e}{\epsilon}$ with ϵ representing the electrical permittivity of the solution. The electric potential is the sum of two different contributions, $\Phi = \phi + \psi$, one generated by the electrodes, placed at the inlet and outlet of the flow geometry, ϕ, and the other, ψ, associated to the charge spontaneously acquired by the fluid near the walls. The imposed potential is described by a Laplace equation, $\nabla^2\phi = 0$, while the induced potential is given by a Poisson equation, $\nabla^2\psi = -\frac{\rho_e}{\epsilon}$.

In many circumstances, when the flow (and the ionic distribution) is steady, the electric double layers are thin and do not overlap at the center of the channel, significant variations of ψ occur only in the normal direction to the channel walls, and a stable Boltzmann distribution of ions in the electric double layer can be assumed. In this situation, the net electric charge density in the fluid, ρ_e, can be obtained by the Boltzmann distribution (see Ref. 1),

$$\rho_e = -2n_o ez \sinh\left(\frac{ez}{k_B T}\psi\right), \tag{5}$$

where n_o is the ion density ($n_o = CN_A$ is the bulk number concentration of ions in the electrolyte solution, C is the molar concentration of ions, and N_A is Avogadro's number), T is the absolute temperature, k_B is the Boltzmann constant, e is the elementary charge, and z is the valence of the ions. In order to obtain the velocity field, first we need to solve for the net charge density distribution (ρ_e). The charge density field can be calculated by combining the Poisson equation for the induced potential equation, which for fully developed steady flow reduces to

$$\frac{\mathrm{d}^2\psi}{\mathrm{d}y^2} = -\frac{\rho_e}{\epsilon}, \tag{6}$$

and the Boltzmann equation (5) to obtain the well-known Poisson–Boltzmann equation,

$$\frac{\mathrm{d}^2\psi}{\mathrm{d}y^2} = \frac{2n_o ez}{\epsilon}\sinh\left(\frac{ez}{k_B T}\psi\right). \tag{7}$$

For a channel flow with electrically charged walls and an applied potential difference between the channel inlet and outlet, a longitudinal electric field is generated that exerts a body force on the counter-ions of the EDL, which move along the channel dragging the neutral liquid core. In general, the distribution of the charged species in the domain is governed by the potential at the walls and by the externally applied electric field. However, when the EDL thickness is small and the potential at the walls is not large, this distribution is essentially governed by the potential at the wall, and the charge distribution near the walls can be determined independently of the applied external electric field. In this work, the charge redistribution is considered to be exactly null as is also the inertial term of the momentum equation, since electro-osmotic (EO) flows are typically slow. Then, for small values of ψ, it is also possible to conduct further simplifications by invoking the Debye–Hückel linearization principle.[1,35,36] Under this approximation ($\sinh x \approx x$), in Eq. (7), $ez\zeta/k_B T$ is assumed small (ζ is the maximum value of ψ at the wall), which is synonymous of a small ratio of electrical to thermal energies, i.e., we assume that the temperature effect on the potential distribution is negligible. In practical terms, involving say a z_+- z_- electrolyte in water, at ambient temperature this implies a zeta potential of less than about 26 mV to have $\frac{ez\zeta}{k_B T} \sim 1$.

Under the Debye–Hückel assumption, the Poisson–Boltzmann equation for the channel flow becomes

$$\frac{\mathrm{d}^2\psi}{\mathrm{d}y^2} = \kappa^2\psi, \tag{8}$$

where $\kappa^2 = \frac{2n_o e^2 z^2}{\epsilon k_B T}$ is the Debye–Hückel parameter, related with the thickness of the Debye layer, $\xi = \frac{1}{\kappa}$ (normally referred to as the EDL thickness).

The induced electric field, ψ, is then given by

$$\psi = \zeta \frac{\cosh(\kappa y)}{\cosh(\kappa H)} \tag{9}$$

for $0 \leq |y| \leq H$ (see Fig. 1) and the corresponding net charge density distribution is

$$\rho_e = -\epsilon \zeta \kappa^2 \frac{\cosh(\kappa y)}{\cosh(\kappa H)}. \tag{10}$$

For more details on the derivation of these equations, refer to Afonso *et al.*[18] and Bruus.[1]

III. RESULTS AND DISCUSSION

The momentum equation, Eq. (2), for a fully developed channel flow reduces to

$$\frac{\mathrm{d}\tau_{xy}}{\mathrm{d}y} = -\rho_e E_x + p_{,x}, \tag{11}$$

where $p_{,x}$ is the streamwise pressure gradient ($p_{,x} = \mathrm{d}p/\mathrm{d}x$) and $E_x \equiv -\mathrm{d}\phi/\mathrm{d}x$ is the imposed constant streamwise gradient of electric potential under fully developed flow conditions. Regardless of the selected viscoelastic model, Eq. (11) can be integrated yielding the following shear stress distribution across the channel:

$$\tau_{xy} = \epsilon \zeta E_x \kappa \frac{\sinh(\kappa y)}{\cosh(\kappa H)} + p_{,x} y. \tag{12}$$

A. PTT models

For the simplified PTT model (sPTT), the extra-stress components that result from application of this constitutive equation to the unidirectional flow of Fig. 1 are given by

$$f(\tau_{kk})\tau_{xx} = 2\lambda \frac{du}{dy}\tau_{xy}, \tag{13}$$

$$f(\tau_{kk})\tau_{xy} = \eta \frac{du}{dy}, \tag{14}$$

where the trace of $\boldsymbol{\tau}$ is $\tau_{kk} = \tau_{xx}$ since τ_{yy} and τ_{zz} are zero,[30] and $\frac{du}{dy}$ is the velocity gradient. Upon division of Eq. (13) by Eq. (14) the following relation between the normal and shear stresses is obtained:

$$\tau_{xx} = 2\frac{\lambda}{\eta}\tau_{xy}^2, \tag{15}$$

leading to the following transverse distribution of the normal stress:

$$\tau_{xx} = 2\frac{\lambda}{\eta}\left(\epsilon \zeta E_x \kappa \frac{\sinh(\kappa y)}{\cosh(\kappa H)} + p_{,x} y\right)^2. \tag{16}$$

Combining Eqs. (12), (14), and (16) allows obtaining the following explicit equations for the normalized velocity gradient for the quadratic and exponential PTT models (cf. Eq. (4)), respectively,

$$\frac{\mathrm{d}(u/u_{sh})}{\mathrm{d}(y/H)} \equiv \frac{\mathrm{d}\bar{u}}{\mathrm{d}\bar{y}} = \left[1 + 2\frac{\varepsilon Wi_\kappa^2}{\bar{\kappa}^2}\left(\Gamma\bar{y} - \bar{\kappa}\frac{\sinh(\bar{\kappa}\bar{y})}{\cosh(\bar{\kappa})}\right)^2\left(1 + \frac{\varepsilon Wi_\kappa^2}{\bar{\kappa}^2}\left(\Gamma\bar{y} - \bar{\kappa}\frac{\sinh(\bar{\kappa}\bar{y})}{\cosh(\bar{\kappa})}\right)^2\right)\right]\left(\Gamma\bar{y} - \bar{\kappa}\frac{\sinh(\bar{\kappa}\bar{y})}{\cosh(\bar{\kappa})}\right), \tag{17}$$

$$\frac{\mathrm{d}(u/u_{sh})}{\mathrm{d}(y/H)} \equiv \frac{\mathrm{d}\bar{u}}{\mathrm{d}\bar{y}} = \left[\exp\left(2\frac{\varepsilon Wi_\kappa^2}{\bar{\kappa}^2}\left(\Gamma\bar{y} - \bar{\kappa}\frac{\sinh(\bar{\kappa}\bar{y})}{\cosh(\bar{\kappa})}\right)^2\right)\right]\left(\Gamma\bar{y} - \bar{\kappa}\frac{\sinh(\bar{\kappa}\bar{y})}{\cosh(\bar{\kappa})}\right), \tag{18}$$

where u_{sh} is the Helmholtz-Smoluchowski electro-osmotic velocity, defined as $u_{sh} = -\frac{\epsilon\zeta E_x}{\eta}$, $Wi_\kappa = \frac{\lambda u_{sh}}{\xi} = \lambda\kappa u_{sh}$ is the Weissenberg number, $\bar{u} = u/u_{sh}$, $\bar{y} = y/H$, $\bar{\kappa} = \kappa H$, and the dimensionless

parameter $\Gamma = -\frac{H^2}{\epsilon\zeta}\left(\frac{p_{,x}}{E_x}\right)$ represents the ratio of pressure to electro-osmotic driving forcings. The velocity profiles for each model can be obtained from integration of the corresponding velocity gradient profile subjected to the no-slip boundary condition at the top (+) or bottom (-) walls, $\bar{u}(\pm 1) = 0$,

$$\bar{u}(\bar{y}) = -\int_{\bar{y}}^{1} f(\bar{y})\, d\bar{y} = F(\bar{y}) - F(1), \tag{19}$$

where $f(\bar{y})$ represents the right-hand-side of Eqs. (17) and (18) and $F(\bar{y})$ represents the integral of $f(\bar{y})$. For the linear stress function, the reader is referred to the works of Afonso *et al.*[18,23] for the velocity profiles for the simplified PTT models, without and with a solvent viscosity contribution, respectively.

1. Quadratic PTT model

For the quadratic sPTT model, the final expression of the dimensionless velocity profile, $\bar{u}(\bar{y})$, is given by

$$\begin{aligned}
\bar{u}(\bar{y}) = 1 &+ \frac{6\Gamma^2\varepsilon\left(\bar{\kappa}^2+2\right)Wi_\kappa^2}{\bar{\kappa}^4} + \frac{10\Gamma^4\varepsilon^2\left(\bar{\kappa}^4+12\bar{\kappa}^2+24\right)Wi_\kappa^4}{\bar{\kappa}^8} - \frac{\Gamma\left(3\bar{\kappa}^4+2\Gamma^4\varepsilon^2Wi_\kappa^4+3\Gamma^2\varepsilon\bar{\kappa}^2Wi_\kappa^2\right)}{6\bar{\kappa}^4} + \\
&\frac{\Gamma\bar{y}^2\left(3\bar{\kappa}^4+2\Gamma^4\varepsilon^2Wi_\kappa^4\bar{y}^4+3\Gamma^2\varepsilon\bar{\kappa}^2Wi_\kappa^2\bar{y}^2\right)}{6\bar{\kappa}^4} - \frac{5\Gamma\varepsilon^2Wi_\kappa^4\mathrm{sech}^4(\bar{\kappa})\cosh(4\bar{\kappa}\bar{y})}{64\bar{\kappa}^2} + \\
&\mathrm{sech}^5(\bar{\kappa})\left(\frac{-5\varepsilon^2Wi_\kappa^4\cosh(3\bar{\kappa})}{24} + \frac{\varepsilon^2Wi_\kappa^4\cosh(5\bar{\kappa})}{40} + \frac{5\varepsilon^2Wi_\kappa^4\cosh(3\bar{\kappa}\bar{y})}{24} - \frac{\varepsilon^2Wi_\kappa^4\cosh(5\bar{\kappa}\bar{y})}{40}\right) + \\
&\cosh(\bar{\kappa}\bar{y})\left(-\frac{5\varepsilon^2Wi_\kappa^4\mathrm{sech}^5(\bar{\kappa})}{4} + \mathrm{sech}^3(\bar{\kappa})\left(\frac{15\Gamma^2\varepsilon^2Wi_\kappa^4\left(\bar{\kappa}^2\bar{y}^2+2\right)}{\kappa^4} + \frac{3\varepsilon Wi_\kappa^2}{2}\right)\right) + \\
&\cosh(\bar{\kappa}\bar{y})\left(\mathrm{sech}(\bar{\kappa})\left(-\frac{10\Gamma^4\varepsilon^2Wi_\kappa^4\left(\bar{\kappa}^4\bar{y}^4+12\bar{\kappa}^2\bar{y}^2+24\right)}{\bar{\kappa}^8} - \frac{6\Gamma^2\varepsilon Wi_\kappa^2\left(\bar{\kappa}^2\bar{y}^2+2\right)}{\bar{\kappa}^4} - 1\right)\right) + \\
&\mathrm{sech}(\bar{\kappa})\sinh(\bar{\kappa}\bar{y})\left(\frac{40\Gamma^4\varepsilon^2Wi_\kappa^4\bar{y}\left(\bar{\kappa}^2\bar{y}^2+6\right)}{\bar{\kappa}^7} + \frac{12\Gamma^2\varepsilon Wi_\kappa^2\bar{y}}{\bar{\kappa}^3}\right) + \\
&\mathrm{sech}^3(\bar{\kappa})\left(-\frac{10\Gamma^2\varepsilon^2Wi_\kappa^4\sinh(3\bar{\kappa})}{9\bar{\kappa}^3} + \frac{10\Gamma^2\varepsilon^2Wi_\kappa^4\bar{y}\sinh(3\bar{\kappa}\bar{y})}{9\bar{\kappa}^3} - \frac{30\Gamma^2\varepsilon^2Wi_\kappa^4\bar{y}\sinh(\bar{\kappa}\bar{y})}{\bar{\kappa}^3}\right) + \\
&\mathrm{sech}^3(\bar{\kappa})\left(\cosh(3\bar{\kappa})\left(\frac{5\Gamma^2\varepsilon^2\left(9\bar{\kappa}^2+2\right)Wi_\kappa^4}{27\bar{\kappa}^4} + \frac{\varepsilon Wi_\kappa^2}{6}\right) + \cosh(3\bar{\kappa}\bar{y})\left(-\frac{5\Gamma^2\varepsilon^2Wi_\kappa^4\left(9\bar{\kappa}^2\bar{y}^2+2\right)}{27\bar{\kappa}^4} - \frac{\varepsilon Wi_\kappa^2}{6}\right)\right) + \\
&\mathrm{sech}^4(\bar{\kappa})\left(\frac{5\Gamma\varepsilon^2Wi_\kappa^4\cosh(4\bar{\kappa})}{64\bar{\kappa}^2} - \frac{5\Gamma\varepsilon^2Wi_\kappa^4\cosh(2\bar{\kappa})}{4\bar{\kappa}^2} + \frac{5\Gamma\varepsilon^2Wi_\kappa^4\sinh(2\bar{\kappa})}{2\bar{\kappa}} - \frac{5\Gamma\varepsilon^2Wi_\kappa^4\sinh(4\bar{\kappa})}{16\bar{\kappa}} - \frac{15}{8}\Gamma\varepsilon^2Wi_\kappa^4\right) + \\
&\mathrm{sech}^4(\bar{\kappa})\left(\frac{5\varepsilon^2Wi_\kappa^4}{4} + \frac{15}{8}\Gamma\varepsilon^2Wi_\kappa^4\bar{y}^2 + \frac{5\Gamma\varepsilon^2Wi_\kappa^4\cosh(2\bar{\kappa}\bar{y})}{4\bar{\kappa}^2} + \frac{5\Gamma\varepsilon^2Wi_\kappa^4\bar{y}\sinh(4\bar{\kappa}\bar{y})}{16\bar{\kappa}} - \frac{5\Gamma\varepsilon^2Wi_\kappa^4\bar{y}\sinh(2\bar{\kappa}\bar{y})}{2\bar{\kappa}}\right) \\
&- \frac{12\Gamma^2\varepsilon Wi_\kappa^2\tanh(\bar{\kappa})}{\bar{\kappa}^3} - \frac{40\Gamma^4\varepsilon^2\left(\bar{\kappa}^2+6\right)Wi_\kappa^4\tanh(\bar{\kappa})}{\bar{\kappa}^7} + \\
&\mathrm{sech}^2(\bar{\kappa})\left(\frac{5\Gamma^3\varepsilon^2\left(6\bar{\kappa}^2+3\right)Wi_\kappa^4\cosh(2\bar{\kappa})}{4\bar{\kappa}^6} + \frac{30\Gamma^2\varepsilon^2Wi_\kappa^4\tanh(\bar{\kappa})}{\bar{\kappa}^3} - \frac{15\Gamma^2\varepsilon^2\left(\bar{\kappa}^2+2\right)Wi_\kappa^4}{\bar{\kappa}^4} - \frac{5\Gamma^3\varepsilon^2Wi_\kappa^4\left(6\bar{\kappa}^2\bar{y}^2+3\right)\cosh(2\bar{\kappa}\bar{y})}{4\bar{\kappa}^6}\right) + \\
&\mathrm{sech}^2(\bar{\kappa})\left(\frac{\Gamma\varepsilon Wi_\kappa^2\left(3\bar{\kappa}^2+5\Gamma^2\varepsilon Wi_\kappa^2\right)}{2\bar{\kappa}^2} + \frac{3\Gamma\varepsilon Wi_\kappa^2\cosh(2\bar{\kappa})}{4\bar{\kappa}^2} - \frac{3\varepsilon Wi_\kappa^2}{2} - \frac{\Gamma\varepsilon Wi_\kappa^2\bar{y}^2\left(3\bar{\kappa}^2+5\Gamma^2\varepsilon Wi_\kappa^2\bar{y}^2\right)}{2\bar{\kappa}^2} - \frac{3\Gamma\varepsilon Wi_\kappa^2\cosh(2\bar{\kappa}\bar{y})}{4\bar{\kappa}^2}\right) + \\
&\mathrm{sech}^2(\bar{\kappa})\left(\sinh(2\bar{\kappa})\left(-\frac{5\Gamma^3\varepsilon^2\left(2\bar{\kappa}^2+3\right)Wi_\kappa^4}{2\bar{\kappa}^5} - \frac{3\Gamma\varepsilon Wi_\kappa^2}{2\bar{\kappa}}\right) + \sinh(2\bar{\kappa}\bar{y})\left(\frac{5\Gamma^3\varepsilon^2Wi_\kappa^4\bar{y}\left(2\bar{\kappa}^2\bar{y}^2+3\right)}{2\bar{\kappa}^5} + \frac{3\Gamma\varepsilon Wi_\kappa^2\bar{y}}{2\bar{\kappa}}\right)\right).
\end{aligned} \tag{20}$$

For the inverse problem (determination of the ratio of forcings, Γ, for a given dimensionless flow rate, $\bar{Q}$), the velocity profile must be integrated,

$$\bar{Q} = \frac{Q}{2Hu_{sh}} = \frac{U}{u_{sh}} = \int_0^1 \bar{u}(\bar{y})\,\mathrm{d}\bar{y}, \tag{21}$$

resulting in the following implicit equation for Γ:

$$a_5\Gamma^5 + a_4\Gamma^4 + a_3\Gamma^3 + a_2\Gamma^2 + a_1\Gamma + a_0 = 0 \tag{22}$$

with coefficients,

$$
\begin{aligned}
a_5 &= -\frac{2\varepsilon^2 W i_\kappa^4}{7\bar{\kappa}^4},\\
a_4 &= \frac{240\varepsilon^2 W i_\kappa^4(\bar{\kappa}-\tanh(\bar{\kappa}))}{\bar{\kappa}^9} - \frac{240\varepsilon^2 W i_\kappa^4\tanh(\bar{\kappa})}{\bar{\kappa}^9} + \frac{240\varepsilon^2 W i_\kappa^4}{\bar{\kappa}^8} - \frac{240\varepsilon^2 W i_\kappa^4\tanh(\bar{\kappa})}{\bar{\kappa}^7} + \frac{120\varepsilon^2 W i_\kappa^4}{\bar{\kappa}^6} - \frac{40\varepsilon^2 W i_\kappa^4\tanh(\bar{\kappa})}{\bar{\kappa}^5}\\
&+ \frac{10\varepsilon^2 W i_\kappa^4}{\bar{\kappa}^4} + \frac{40\varepsilon^2 W i_\kappa^4\left(\bar{\kappa}\left(\bar{\kappa}^2+6\right)-3\left(\bar{\kappa}^2+2\right)\tanh(\bar{\kappa})\right)}{\bar{\kappa}^9} - \frac{120\varepsilon^2 W i_\kappa^4\left(\left(\bar{\kappa}^2+2\right)\tanh(\bar{\kappa})-2\bar{\kappa}\right)}{\bar{\kappa}^9}\\
&- \frac{10\varepsilon^2 W i_\kappa^4\left(\left(\bar{\kappa}^4+12\bar{\kappa}^2+24\right)\tanh(\bar{\kappa})-4\bar{\kappa}\left(\bar{\kappa}^2+6\right)\right)}{\bar{\kappa}^9},\\
a_3 &= \frac{15\varepsilon^2 W i_\kappa^4\left(\bar{\kappa}+\bar{\kappa}\tanh^2(\bar{\kappa})-\tanh(\bar{\kappa})\right)}{4\bar{\kappa}^7} - \frac{15\varepsilon^2 W i_\kappa^4\tanh(\bar{\kappa})}{4\bar{\kappa}^7} + \frac{15\varepsilon^2 W i_\kappa^4\cosh(2\bar{\kappa})\mathrm{sech}^2(\bar{\kappa})}{4\bar{\kappa}^6} - \frac{15\varepsilon^2 W i_\kappa^4\sinh(2\bar{\kappa})\mathrm{sech}^2(\bar{\kappa})}{2\bar{\kappa}^5}\\
&+ \frac{15\varepsilon^2 W i_\kappa^4\cosh(2\bar{\kappa})\mathrm{sech}^2(\bar{\kappa})}{2\bar{\kappa}^4} - \frac{5\varepsilon^2 W i_\kappa^4\sinh(2\bar{\kappa})\mathrm{sech}^2(\bar{\kappa})}{\bar{\kappa}^3} + \frac{2\varepsilon^2 W i_\kappa^4\mathrm{sech}^2(\bar{\kappa})}{\bar{\kappa}^2}\\
&+ \frac{15\varepsilon^2 W i_\kappa^4\left(\tanh(\bar{\kappa})\left(-2\bar{\kappa}^2+\bar{\kappa}\tanh(\bar{\kappa})-1\right)+\bar{\kappa}\right)}{4\bar{\kappa}^7} + \frac{5\varepsilon^2 W i_\kappa^4\mathrm{sech}^2(\bar{\kappa})\left(2\bar{\kappa}\left(2\bar{\kappa}^2+3\right)\cosh(2\bar{\kappa})-3\left(2\bar{\kappa}^2+1\right)\sinh(2\bar{\kappa})\right)}{8\bar{\kappa}^7} - \frac{2\varepsilon W i_\kappa^2}{5\bar{\kappa}^2},\\
a_2 &= -\frac{10\varepsilon^2 W i_\kappa^4\sinh(3\bar{\kappa})\mathrm{sech}^3(\bar{\kappa})}{81\bar{\kappa}^5} + \frac{30\varepsilon^2 W i_\kappa^4\tanh(\bar{\kappa})\mathrm{sech}^2(\bar{\kappa})}{\bar{\kappa}^5} - \frac{30\varepsilon^2 W i_\kappa^4(\bar{\kappa}-\tanh(\bar{\kappa}))\mathrm{sech}^2(\bar{\kappa})}{\bar{\kappa}^5}\\
&- \frac{10\varepsilon^2 W i_\kappa^4\mathrm{sech}^3(\bar{\kappa})(\sinh(3\bar{\kappa})-3\kappa\cosh(3\bar{\kappa}))}{81\bar{\kappa}^5} - \frac{30\varepsilon^2 W i_\kappa^4\mathrm{sech}^2(\bar{\kappa})}{\bar{\kappa}^4} + \frac{10\varepsilon^2 W i_\kappa^4\cosh(3\bar{\kappa})\mathrm{sech}^3(\bar{\kappa})}{27\bar{\kappa}^4}\\
&- \frac{10\varepsilon^2 W i_\kappa^4\sinh(3\bar{\kappa})\mathrm{sech}^3(\bar{\kappa})}{9\bar{\kappa}^3} + \frac{30\varepsilon^2 W i_\kappa^4\tanh(\bar{\kappa})\mathrm{sech}^2(\bar{\kappa})}{\bar{\kappa}^3} - \frac{15\varepsilon^2 W i_\kappa^4\mathrm{sech}^2(\bar{\kappa})}{\bar{\kappa}^2} + \frac{5\varepsilon^2 W i_\kappa^4\cosh(3\bar{\kappa})\mathrm{sech}^3(\bar{\kappa})}{3\bar{\kappa}^2}\\
&+ \frac{15\varepsilon^2 W i_\kappa^4\left(\left(\bar{\kappa}^2+2\right)\tanh(\bar{\kappa})-2\bar{\kappa}\right)\mathrm{sech}^2(\bar{\kappa})}{\bar{\kappa}^5} - \frac{5\varepsilon^2 W i_\kappa^4\mathrm{sech}^3(\bar{\kappa})\left(\left(9\bar{\kappa}^2+2\right)\sinh(3\bar{\kappa})-6\kappa\cosh(3\bar{\kappa})\right)}{81\bar{\kappa}^5} + \frac{12\varepsilon W i_\kappa^2(\bar{\kappa}-\tanh(\bar{\kappa}))}{\bar{\kappa}^5}\\
&- \frac{12\varepsilon W i_\kappa^2\tanh(\bar{\kappa})}{\bar{\kappa}^5} + \frac{12\varepsilon W i_\kappa^2}{\bar{\kappa}^4} - \frac{12\varepsilon W i_\kappa^2\tanh(\bar{\kappa})}{\bar{\kappa}^3} + \frac{6\varepsilon W i_\kappa^2}{\bar{\kappa}^2} - \frac{6\varepsilon W i_\kappa^2\left(\left(\bar{\kappa}^2+2\right)\tanh(\bar{\kappa})-2\bar{\kappa}\right)}{\bar{\kappa}^5},\\
a_1 &= -\frac{5\varepsilon^2 W i_\kappa^4\sinh(4\bar{\kappa})\mathrm{sech}^4(\bar{\kappa})}{256\bar{\kappa}^3} + \frac{5\varepsilon^2 W i_\kappa^4\tanh(\bar{\kappa})\mathrm{sech}^2(\bar{\kappa})}{4\bar{\kappa}^3} + \frac{5\varepsilon^2 W i_\kappa^4\mathrm{sech}^4(\bar{\kappa})(\sinh(2\bar{\kappa})-2\bar{\kappa}\cosh(2\bar{\kappa}))}{8\bar{\kappa}^3}\\
&- \frac{5\varepsilon^2 W i_\kappa^4\mathrm{sech}^4(\bar{\kappa})(\sinh(4\bar{\kappa})-4\bar{\kappa}\cosh(4\bar{\kappa}))}{256\bar{\kappa}^3} + \frac{5\varepsilon^2 W i_\kappa^4\cosh(4\bar{\kappa})\mathrm{sech}^4(\bar{\kappa})}{64\bar{\kappa}^2} - \frac{5\varepsilon^2 W i_\kappa^4\cosh(2\bar{\kappa})\mathrm{sech}^4(\bar{\kappa})}{4\bar{\kappa}^2}\\
&- \frac{5}{4}\varepsilon^2 W i_\kappa^4\mathrm{sech}^4(\bar{\kappa}) + \frac{5\varepsilon^2 W i_\kappa^4\sinh(2\bar{\kappa})\mathrm{sech}^4(\bar{\kappa})}{2\bar{\kappa}} - \frac{5\varepsilon^2 W i_\kappa^4\sinh(4\bar{\kappa})\mathrm{sech}^4(\bar{\kappa})}{16\bar{\kappa}} + \frac{3\varepsilon W i_\kappa^2\left(\bar{\kappa}+\bar{\kappa}\tanh^2(\bar{\kappa})-\tanh(\bar{\kappa})\right)}{4\bar{\kappa}^3}\\
&- \frac{3\varepsilon W i_\kappa^2\tanh(\bar{\kappa})}{4\bar{\kappa}^3} + \frac{3\varepsilon W i_\kappa^2\cosh(2\bar{\kappa})\mathrm{sech}^2(\bar{\kappa})}{4\bar{\kappa}^2} + \varepsilon W i_\kappa^2\mathrm{sech}^2(\bar{\kappa}) - \frac{3\varepsilon W i_\kappa^2\sinh(2\bar{\kappa})\mathrm{sech}^2(\bar{\kappa})}{2\bar{\kappa}} - \frac{1}{3},\\
a_0 &= 1 - \frac{3}{2}\varepsilon W i_\kappa^2\mathrm{sech}^2(\bar{\kappa}) + \frac{1}{6}\varepsilon W i_\kappa^2\cosh(3\bar{\kappa})\mathrm{sech}^3(\bar{\kappa}) + \frac{5}{4}\varepsilon^2 W i_\kappa^4\mathrm{sech}^4(\bar{\kappa}) - \frac{5}{24}\varepsilon^2 W i_\kappa^4\cosh(3\bar{\kappa})\mathrm{sech}^5(\bar{\kappa})\\
&+ \frac{1}{40}\varepsilon^2 W i_\kappa^4\cosh(5\bar{\kappa})\mathrm{sech}^5(\bar{\kappa}) - \frac{\varepsilon W i_\kappa^2\sinh(3\bar{\kappa})\mathrm{sech}^3(\bar{\kappa})}{18\bar{\kappa}} + \frac{5\varepsilon^2 W i_\kappa^4\sinh(3\bar{\kappa})\mathrm{sech}^5(\bar{\kappa})}{72\bar{\kappa}} - \frac{\varepsilon^2 W i_\kappa^4\sinh(5\bar{\kappa})\mathrm{sech}^5(\bar{\kappa})}{200\bar{\kappa}}\\
&- \frac{\tanh(\bar{\kappa})}{\bar{\kappa}} + \frac{3\varepsilon W i_\kappa^2\tanh(\bar{\kappa})\mathrm{sech}^2(\bar{\kappa})}{2\bar{\kappa}} - \frac{5\varepsilon^2 W i_\kappa^4\tanh(\bar{\kappa})\mathrm{sech}^4(\bar{\kappa})}{4\bar{\kappa}} - \bar{Q}.
\end{aligned}
\tag{23}
$$

Although we do not give a closed form explicit solution for Γ, the correct solution can be obtained based on the physical assumptions of the problem considered. For the special case of pure pressure-driven flow, the velocity profile is given by

$$
\frac{u}{U} = \bar{p}_{,x}^5\left(\frac{1}{3}\varepsilon^2 Wi^4\bar{y}^6 - \frac{\varepsilon^2 Wi^4}{3}\right) + \bar{p}_{,x}^3\left(\frac{1}{2}\varepsilon Wi^2\bar{y}^4 - \frac{\varepsilon Wi^2}{2}\right) + \bar{p}_{,x}\left(\frac{\bar{y}^2}{2} - \frac{1}{2}\right) \tag{24}
$$

with the pressure gradient obtained as a solution of the following equation:

$$
-\frac{\bar{p}_{,x}}{3} - \frac{2\varepsilon Wi^2\bar{p}_{,x}^3}{5} - \frac{2\left(\varepsilon Wi^2\right)^2\bar{p}_{,x}^5}{7} - 1 = 0, \tag{25}
$$

where $\bar{p}_{,x} = p_{,x}H^2/(\eta U)$ and $Wi = \lambda U/H$ with U representing the imposed mean velocity. With the help of the Bolzano and intermediate value theorems, the existence of a unique solution, $\bar{p}_{,x}$, for all εWi^2 can be proved.

2. Exponential sPTT model

For the exponential sPTT model, Eq. (19) is still valid, but the analytical solution for the velocity profile could only be obtained for pure electro-osmotic flow ($\Gamma = 0$) and assuming the approximation $\sinh(\bar{\kappa}\bar{y}) \approx \frac{1}{2}\exp(\bar{\kappa}\bar{y})$. This approximation is usually accurate because in most

micro-device applications, the thickness of the electric double layer is very small, about 1–3 orders of magnitude smaller than the width of the microfluidic channel, hence $\bar{\kappa}$ is a large value (also, the Debye–Hückel linearization requires $\bar{\kappa} > 10$); however, close to the centerline ($\bar{y} \sim 0$) the approximation $\sinh(\bar{\kappa}\bar{y}) \approx \frac{1}{2}\exp(\bar{\kappa}\bar{y})$ becomes less adequate.

Three approximate solutions were obtained, depending on the type and degree of approximation used. If we assume $\sinh(\bar{\kappa}\bar{y}) \approx \frac{1}{2}\exp(\bar{\kappa}\bar{y})$ everywhere in Eq. (18), then the velocity profile is given by

$$\bar{u}(\bar{y}) = \frac{\sqrt{\frac{\pi}{2}}\left(\text{erfi}\left[\frac{B\sqrt{A}\exp(\bar{\kappa})}{\sqrt{2}}\right] - \text{erfi}\left[\frac{B\sqrt{A}\exp(\bar{\kappa}|\bar{y}|)}{\sqrt{2}}\right]\right)}{2\bar{\kappa}\sqrt{A}}, \tag{26}$$

where $\text{erfi}(z) = -i\,\text{erf}(iz)$ with $\text{erf}(\cdot)$ denoting the error function, $A = \frac{\varepsilon W i_\kappa^2}{\bar{\kappa}^2}$, and $B = \frac{\bar{\kappa}}{\cosh(\bar{\kappa})}$. It is important to note that with this approximation the solution is no longer symmetric ($\frac{d\bar{u}}{d\bar{y}}_{|\bar{y}=0} \neq 0$ although $\frac{d\bar{u}}{d\bar{y}}_{|\bar{y}=0} \approx 0$ for $\bar{\kappa} > 10$). However, if the approximation $\sinh(\bar{\kappa}\bar{y}) \approx \frac{1}{2}\exp(\bar{\kappa}\bar{y})$ is used only in the argument of the exponential function of Eq. (18), the symmetry is preserved, and the resulting solution is given by

$$\begin{aligned}\bar{u}(\bar{y}) = &-(\exp[-\bar{\kappa}(1+|\bar{y}|)])\left(2B\sqrt{A}\left(\exp\left[\frac{1}{2}B^2A\exp[2\bar{\kappa}|\bar{y}|] + \bar{\kappa}\right] - \exp\left[\frac{1}{2}B^2A\exp[2\bar{\kappa}] + \bar{\kappa}|\bar{y}|\right]\right)\right)\Big/\left(4\bar{\kappa}\sqrt{A}\right) - \\ &\sqrt{2\pi}\left(-1 + B^2A\right)\left(\text{erfi}\left[\frac{B\sqrt{A}\exp[\bar{\kappa}]}{\sqrt{2}}\right] - \text{erfi}\left[\frac{B\sqrt{A}\exp[\bar{\kappa}|\bar{y}|]}{\sqrt{2}}\right]\right)\Big/\left(4\bar{\kappa}\sqrt{A}\right)\end{aligned} \tag{27}$$

which is more accurate than the approximate solution of Eq. (26). For comparison purposes, Eq. (18) was also solved by numerical integration with second order accuracy, using a sufficiently small integration step to achieve high accuracy, and the corresponding numerical solution will be considered as the "exact" solution below,

$$\bar{u}(\bar{y}) = -\int_{\bar{y}}^{1}\left[\exp\left(2\frac{\varepsilon W i_\kappa^2}{\bar{\kappa}^2}\left(\Gamma\bar{y} - \bar{\kappa}\frac{\sinh(\bar{\kappa}\bar{y})}{\cosh(\bar{\kappa})}\right)^2\right)\right]\left(\Gamma\bar{y} - \bar{\kappa}\frac{\sinh(\bar{\kappa}\bar{y})}{\cosh(\bar{\kappa})}\right)d\bar{y}. \tag{28}$$

Fig. 2 compares the velocity profiles obtained by the two approximate analytical solutions with the "exact" numerical solutions, for $\varepsilon W i_\kappa^2 = 0.5$, and $\bar{\kappa} = 100$, 10, and 1. As expected, for the extreme case of $\bar{\kappa} = 1$, corresponding to overlapped EDLs, both analytical solutions diverge from the correct solution, but the solution that preserves the symmetry is more accurate (see Fig. 2(c)). Note that the Debye–Hückel approximation is only valid for non-overlapped EDLs ($\bar{\kappa} > 10$); therefore, as shown in Figs. 2(a) and 2(b), for such values of $\bar{\kappa}$, the solution that does not preserve symmetry (Eq. (26)) is still reasonably well accurate.

An analytic formula for the velocity profile (with $\Gamma \neq 0$) based on the Taylor series expansion of the terms $\left(\Gamma\bar{y} - \bar{\kappa}\frac{\sinh(\bar{\kappa}\bar{y})}{\cosh(\bar{\kappa})}\right)$ and $\left(\Gamma\bar{y} - \bar{\kappa}\frac{\sinh(\bar{\kappa}\bar{y})}{\cosh(\bar{\kappa})}\right)^2$ of Eq. (18) is still possible, but because of the inability of these polynomial functions to represent the exponential growth of $\sinh(\bar{\kappa}\bar{y})$ for large values of $\bar{\kappa}$, the numerical integration is performed instead (as explained above).

Fig. 2(d) shows the velocity profiles obtained by numerical integration for the combined electro-osmotic/pressure-driven flow for $\Gamma = -1$ and 1, where the effect of adverse ($\Gamma > 0$) and favorable ($\Gamma < 0$) pressure gradients is clear.

A comparison between solutions for the linear, quadratic, and the exponential sPTT models is shown in Fig. 3 for $\varepsilon W i_\kappa^2 = 0.5$ and 1.125. When $\varepsilon W i_\kappa^2$ increases, the dimensionless flow rate also increases for the three models. For $\varepsilon W i_\kappa^2 = 0.5$, the exponential and the quadratic sPTT models show similar velocity profiles, but as we increase $\varepsilon W i_\kappa^2$, the exponential model shows higher velocities. This happens because all sPTT models show increasing shear-thinning behavior with increasing $\varepsilon W i_\kappa^2$, due to the non-linearity of the term containing the scalar function, with the linear and quadratic functions approaching less well the exponential function as $\varepsilon W i_\kappa^2$ increases. Since the most nonlinear scalar function is the exponential function, the shear thinning effects are more intense for this model.

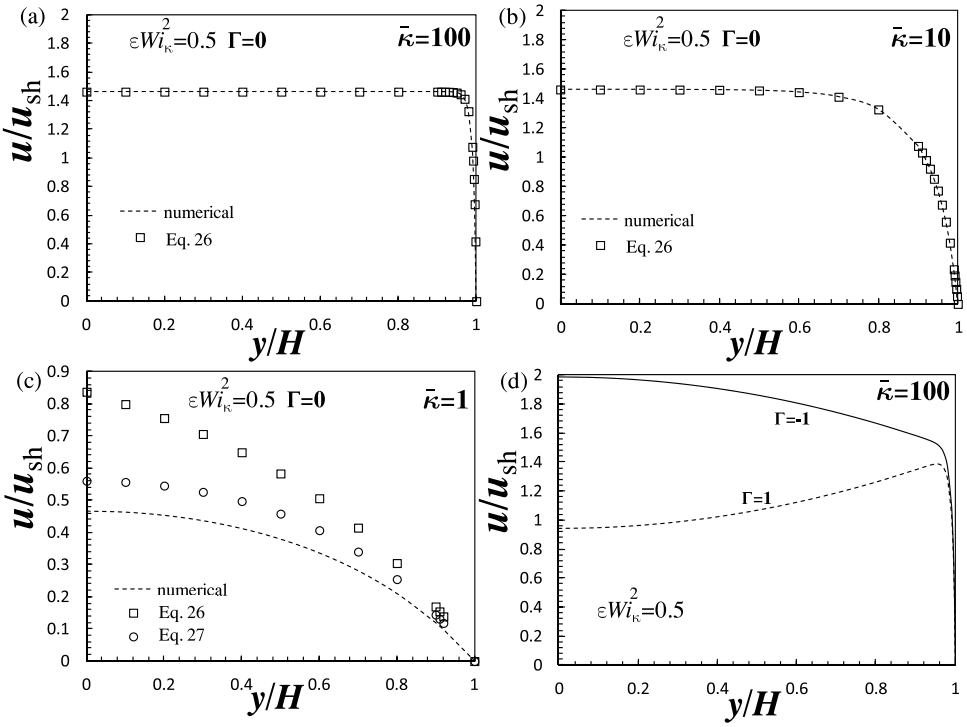

FIG. 2. Dimensionless velocity profiles of pure EO flows ($\Gamma = 0$) for the exponential sPTT model (Eqs. (26)–(28)) for $\varepsilon W i_\kappa^2 = 0.5$ and different values of $\bar{\kappa}$, (a) $\bar{\kappa} = 100$, (b) $\bar{\kappa} = 10$, and (c) $\bar{\kappa} = 1$; and (d) dimensionless velocity profiles computed numerically for the combined electro-osmotic/pressure-driven flow with $\Gamma = -1$ and 1.

The influence of the mixed electro-osmotic/pressure gradient forcings on the stress behavior is presented in Fig. 4(a), where we show the dimensionless shear stress $\bar{\tau}_{xy} = \tau_{xy}/(\eta u_{sh}/H)$ profiles across the channel, at $\Gamma = 0$, 1, and -1, for $\bar{\kappa} = 20$ (for the same forcing, the shear stress is the same for all the selected viscoelastic models). As expected, the shear stress is null at the center of the channel and has a positive or negative slope depending on whether the pressure gradient is adverse ($\Gamma > 0$) or favorable ($\Gamma < 0$), respectively. In the channel core, the variation is linear as is typical of pressure gradient driven flow, and as the wall is approached the shear stress starts to deviate from

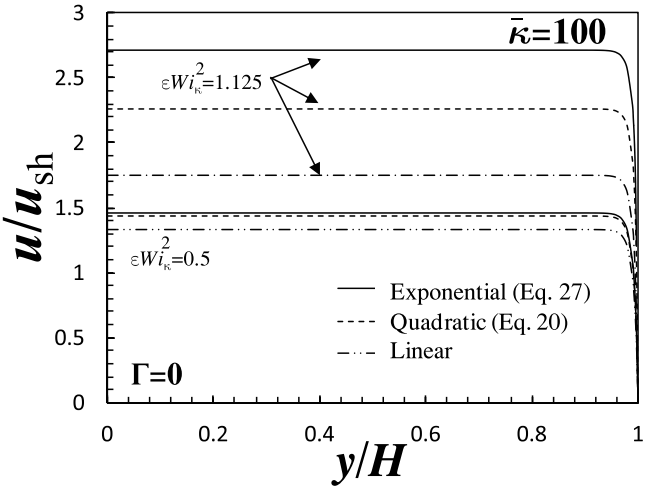

FIG. 3. Dimensionless velocity profiles for the linear, exponential, and quadratic sPTT models for $\varepsilon W i_\kappa^2 = 0.5$ and $\varepsilon W i_\kappa^2 = 1.125$, with $\Gamma = 0$ and $\bar{\kappa} = 100$.

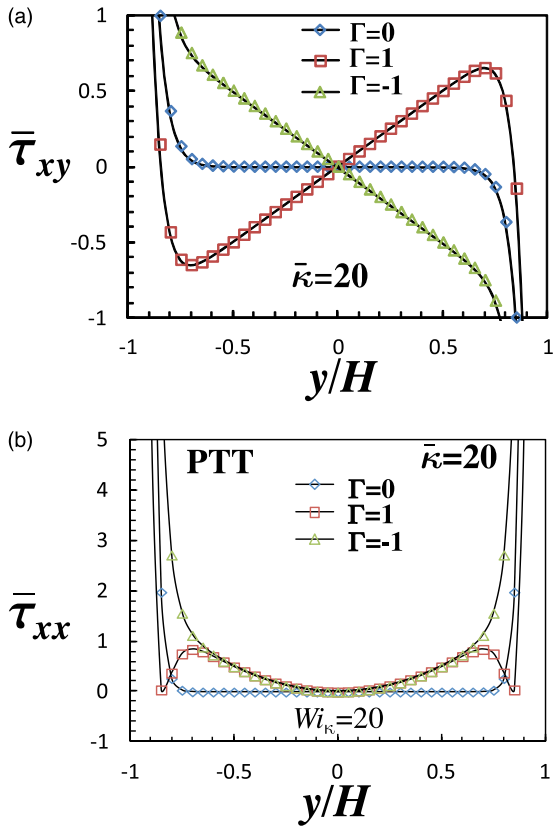

FIG. 4. Dimensionless shear and normal stress profiles across the channel for three different values of Γ and $\bar{\kappa} = 20$: (a) shear stress $\bar{\tau}_{xy}$ and (b) normal stress $\bar{\tau}_{xx}$ at $Wi_{\kappa} = 20$.

its linear variation due to the sharp velocity gradients associated with the EO forcing. Regarding the dimensionless normal stress, $\bar{\tau}_{xx} = \frac{\tau_{xx}H}{(\eta u_{sh})}$ (see Figure 4(b), for the sPTT) we can see that, the intense effects of the electric field near the wall promote a large increase of the normal stress, as it varies with the square of the shear stress. Therefore, at the core of the channel, it tends to be small (it becomes null for $\Gamma = 0$), and near the wall it drastically increases.

As found for the shear stress, the behavior at the core of the channel is essentially determined by the pressure gradient forcing, with the electro-osmotic forcing affecting the normal stress profiles near the wall. This is well shown in the comparison between the two profiles for $|\Gamma| = 1$, consisting of an adverse ($\Gamma = 1$) and favorable ($\Gamma = -1$) forcings.

Near the walls, the normal stress behavior is dramatically different because in one case the EO forcing acts in the same direction as the pressure forcing and the normal stress continues to rise as the wall is approached; whereas in the other case, the EO forcing acts in the opposite direction leading to a non-monotonic behavior of the stress.

B. Johnson-Segalman model

For the fully developed flow of a viscoelastic fluid described by the Johnson-Segalman model, the stress components are given by[27,32]

$$\tau_{xx} = \lambda \frac{du}{dy} \tau_{xy} (a + 1), \tag{29}$$

$$\tau_{yy} = \lambda \frac{du}{dy} \tau_{xy} (a - 1), \tag{30}$$

$$\tau_{xy} = \eta \frac{du}{dy} + \frac{\lambda}{2}\frac{du}{dy}\tau_{xx}(a-1) + \frac{\lambda}{2}\frac{du}{dy}\tau_{yy}(a+1). \tag{31}$$

A combination of Eqs. (29)–(31) and (12) gives the following differential equation for the velocity gradient:

$$\lambda^2\left(\epsilon\zeta E_x\kappa\frac{\sinh(\kappa y)}{\cosh(\kappa H)} + p_{,x}y\right)(a^2-1)\left(\frac{du}{dy}\right)^2 + \eta\frac{du}{dy} = \epsilon\zeta E_x\kappa\frac{\sinh(\kappa y)}{\cosh(\kappa H)} + p_{,x}y. \tag{32}$$

This is a non-linear, first-order, and non-homogeneous differential equation and it can be written in dimensionless form as

$$\frac{Wi_\kappa^2}{\bar{\kappa}^2}\left(\Gamma\bar{y} - \bar{\kappa}\frac{\sinh(\bar{\kappa}\bar{y})}{\cosh(\bar{\kappa})}\right)(a^2-1)\left(\frac{\mathrm{d}\bar{u}}{\mathrm{d}\bar{y}}\right)^2 + \frac{\mathrm{d}\bar{u}}{\mathrm{d}\bar{y}} = \Gamma\bar{y} - \bar{\kappa}\frac{\sinh(\bar{\kappa}\bar{y})}{\cosh(\bar{\kappa})}. \tag{33}$$

For pure electro-osmotic flow ($\Gamma = 0$), an exact solution for this differential equation can be obtained using the no-slip wall boundary condition, $u(1) = 0$, which is given by

$$\begin{aligned}\bar{u}(\bar{y}) \quad &= \frac{\cosh(\bar{\kappa})}{2Wi_\kappa^2(1-a^2)}\left\{\frac{1}{2}\ln\left[\frac{[1+A_1(1)][1-A_1(\bar{y})]}{[1-A_1(1)][1+A_1(\bar{y})]}\right] - \ln\left[\frac{\tanh\left(|\frac{\bar{\kappa}\bar{y}}{2}|\right)}{\tanh\left(\frac{\bar{\kappa}}{2}\right)}\right]\right\} \\ &-\frac{\cosh(\bar{\kappa})}{2Wi_\kappa^2(1-a^2)}\left[\frac{2\sqrt{(1-a^2)Wi_\kappa^2}}{\cosh(\bar{\kappa})}\{\arcsin[A_2(\bar{y})] - \arcsin[A_2(1)]\}\right],\end{aligned} \tag{34}$$

where

$$\begin{aligned}A_1(\bar{y}) &= \frac{\cosh(\bar{\kappa}\bar{y})}{\sqrt{1-4Wi_\kappa^2(1-a^2)\frac{\sinh^2(\bar{\kappa}\bar{y})}{\cosh^2(\bar{\kappa})}}}, \\ A_2(\bar{y}) &= \frac{2\sqrt{(1-a^2)Wi_\kappa^2}\cosh(\bar{\kappa}\bar{y})}{\sqrt{\cosh^2(\bar{\kappa}) + 4Wi_\kappa^2(1-a^2)}}.\end{aligned} \tag{35}$$

For the non-affine PTT model, a more general solution was presented by Dhinakaran *et al.*[22] using the linear form of the scalar function, and their solution reduces to Eq. (34) by taking the limit $\varepsilon \to 0$ and assuming $\xi = 1 - a$ (Eq. (24) of their work).

For the combined electro-osmotic/pressure driven forcing problem, the direct solution is semi-analytical; the shear stress is given by Eq. (12) and then Eq. (33) is numerically solved to compute the velocity profile. For pure pressure-driven flow, the equations have to be renormalized (we use instead $\bar{p}_{,x} = p_{,x}H^2/(\eta U)$, $Wi = \lambda U/H$) using the mean velocity (U) rather than the Helmholtz-Smoluchowski velocity and the corresponding solution is given as a particular case of the analytical solution for the linear PTT model of Alves *et al.*[31] by taking the limit $\varepsilon \to 0$ and assuming $\xi = 1 - a$. For completeness, we presented the solution for this model, but we do not plot or discuss its results since this would not add anything qualitatively different.

C. Giesekus model

For the fully developed flow of a Giesekus fluid, the velocity gradient and normal stress equations are

$$\frac{du}{dy} = \frac{2\alpha\tau_{xy}}{\eta}\frac{\left[1+(2\alpha-1)\sqrt{1-\left(\frac{2\alpha\lambda}{\eta}\tau_{xy}\right)^2}\right]}{\left[(2\alpha-1)+\sqrt{1-\left(\frac{2\alpha\lambda}{\eta}\tau_{xy}\right)^2}\right]^2}, \tag{36}$$

$$\tau_{yy} = \frac{-1+\sqrt{1-\left(\frac{2\alpha\lambda}{\eta}\tau_{xy}\right)^2}}{\frac{2\alpha\lambda}{\eta}}, \tag{37}$$

$$\tau_{xx} = \frac{(1-\alpha)\left[1-\sqrt{1-\left(\frac{2\alpha\lambda}{\eta}\tau_{xy}\right)^2}\right] + 2\alpha^2\left(\frac{\lambda}{\eta}\tau_{xy}\right)^2}{\frac{\alpha\lambda}{\eta}\left[(2\alpha-1)+\sqrt{1-\left(\frac{2\alpha\lambda}{\eta}\tau_{xy}\right)^2}\right]}, \tag{38}$$

with τ_{xy} given by Eq. (12) and with Eq. (36) already written explicitly in order to $\frac{du}{dy}$. For more details on the derivation of these equations, refer to the works of Yoo and Choi[33] and Ferrás *et al.*,[34] which present the solutions for the pure pressure-driven flow. Note that two branches of solutions are possible for the fully developed Giesekus fluid flow, but here only the upper branch is assumed as discussed by Yoo and Choi.[33] Note also that from thermodynamic considerations together with the assumption of a physical solution, we obtain the restrictions, $\tau_{xx} - \tau_{yy} \geq 0$ and $1 - \left(\frac{2\alpha\lambda}{\eta}\tau_{xy}\right)^2 \geq 0$, as discussed by Yoo and Choi.[33]

Assuming the previous normalizations and a pure electro-osmotic flow, the equation for the normalized shear rate is given by

$$\frac{\mathrm{d}\bar{u}}{\mathrm{d}\bar{y}} = -2\alpha\bar{\kappa}\frac{\sinh(\bar{\kappa}\bar{y})}{\cosh(\bar{\kappa})}\frac{\left[1+(2\alpha-1)\sqrt{1-\left(2\alpha Wi_\kappa\frac{\sinh(\bar{\kappa}\bar{y})}{\cosh(\bar{\kappa})}\right)^2}\right]}{\left[(2\alpha-1)+\sqrt{1-\left(2\alpha Wi_\kappa\frac{\sinh(\bar{\kappa}\bar{y})}{\cosh(\bar{\kappa})}\right)^2}\right]^2} \tag{39}$$

with the following restrictions:

$$Wi_\kappa \leq \frac{1}{2\alpha}\coth(\bar{\kappa}) \text{ if } \frac{1}{2} < \alpha \leq 1, \tag{40}$$

$$Wi_\kappa < \sqrt{\frac{1}{\alpha}-1}\coth(\bar{\kappa}) \text{ if } 0 < \alpha \leq \frac{1}{2}. \tag{41}$$

Integration of Eq. (39) assuming no-slip at any of the solid walls, $u(\pm 1) = 0$, results in the following velocity profile, $\bar{u}(\bar{y})$:

$$\bar{u}(\bar{y}) = F(\bar{y}) - F(1) \tag{42}$$

with

$$F(\bar{y}) = \frac{a_G c_G}{d_G^2}\left(-\frac{2\left((2\alpha-1)b_G\left(4\alpha^2-4\alpha-2d_G^2+1\right)+d_G^3\right)\operatorname{arctanh}\left(\frac{(2\alpha-1)\tan\left(\frac{t}{2}\right)+d_G}{\sqrt{-(4\alpha^2-4\alpha-d_G^2+1)}}\right)}{\left[-\left(4\alpha^2-4\alpha-d_G^2+1\right)\right]^{3/2}}\right.$$

$$\left. -\frac{(2\alpha-1)d_G\cos(t)(-2\alpha b_G+b_G+d_G)}{(2\alpha-d_G-1)(2\alpha+d_G-1)(2\alpha+d_G\sin(t)-1)}+b_G t\right),$$

where

$$t = \arcsin\left(\frac{\sqrt{1-\left(\frac{2\alpha Wi_\kappa\sinh(\bar{\kappa}\bar{y})}{\cosh(\bar{\kappa})}\right)^2}}{\sqrt{\operatorname{sech}^2(\bar{\kappa})\left(4\alpha^2Wi_\kappa^2+\cosh^2(\bar{\kappa})\right)}}\right),$$

$$a_G = \cosh(\bar{\kappa})\sqrt{\alpha^2Wi_\kappa^2\operatorname{sech}^2(\bar{\kappa})\left(\frac{\cosh^2(\bar{\kappa})}{4\alpha^2Wi_\kappa^2}+1\right)},$$

$$b_G = 2(2\alpha-1)\sqrt{\alpha^2Wi_\kappa^2\operatorname{sech}^2(\bar{\kappa})\left(\frac{\cosh^2(\bar{\kappa})}{4\alpha^2Wi_\kappa^2}+1\right)},$$

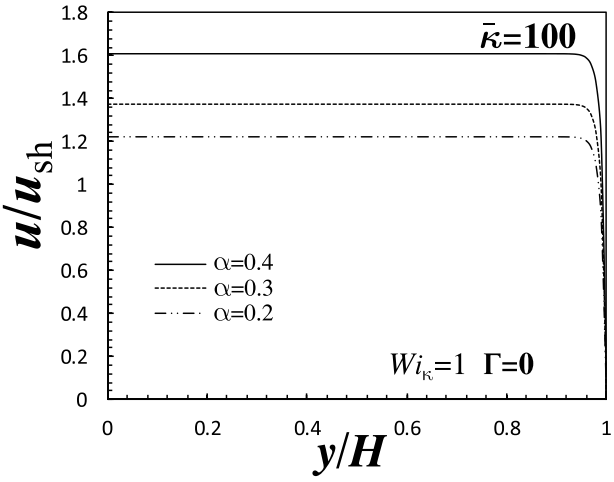

FIG. 5. Dimensionless velocity profiles for pure EOF of a Giesekus fluid (Eq. (43)) for different values of the mobility parameter, α, for $Wi_\kappa = 1$, $\Gamma = 0$, and $\bar{\kappa} = 100$.

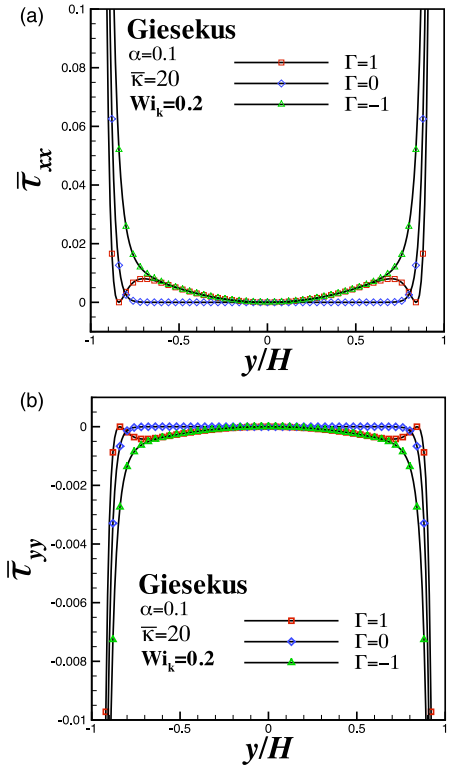

FIG. 6. Variation of the dimensionless normal stresses $\bar{\tau}_{xx}$ and $\bar{\tau}_{yy}$ of the Giesekus model, along the channel width, for $\Gamma = 0, 1$, and -1, $\alpha = 0.1$, $\bar{\kappa} = 20$, and $Wi_\kappa = 0.2$.

$$c_G = \frac{2\sqrt{\alpha^2 Wi_\kappa^2 \operatorname{sech}^2(\bar{\kappa})\left(\frac{\cosh^2(\bar{\kappa})}{4\alpha^2 Wi_\kappa^2}+1\right)}}{\alpha Wi_\kappa^2\sqrt{\frac{\cosh^2(\bar{\kappa})}{4\alpha^2 Wi_\kappa^2}+1}},$$

$$d_G = 2\sqrt{\alpha^2 Wi_\kappa^2 \operatorname{sech}^2(\bar{\kappa})\left(\frac{\cosh^2(\bar{\kappa})}{4\alpha^2 Wi_\kappa^2}+1\right)}. \tag{43}$$

To perform the integration of Eq. (39), two consecutive variable substitutions were used. The first was $s = \sqrt{1 - \left(2\alpha Wi_\kappa \frac{\sinh(\bar{\kappa}\bar{y})}{\cosh(\bar{\kappa})}\right)^2}$ followed by $t = \arcsin\left(\frac{s\cosh(\bar{\kappa})}{\sqrt{4\alpha^2 Wi_\kappa^2 + \cosh^2(\bar{\kappa})}}\right)$.

The velocity profiles for the Giesekus model are plotted in Fig. 5 illustrating an increase of the dimensionless velocity with the increase of the mobility parameter, α.

For the normal stresses, a similar behavior to that discussed for the sPTT was obtained. For the normal stress $\bar{\tau}_{yy}$, similar results are obtained, except that $\bar{\tau}_{yy}$ is negative (see Fig. 6), i.e., there is compression in the y direction. Near the wall this compression increases, leading to an increase of the fluid stretch (positive $\bar{\tau}_{xx}$) in the x direction, as shown before.

IV. CONCLUSIONS

A series of new analytical and semi-analytical solutions were obtained in this work for channel flows of viscoelastic fluids in microchannels under the influence of electrokinetic and pressure forcings using the Debye–Hückel approximation. The viscoelastic models used are the quadratic and the exponential sPTT, the Johnson-Segalman model, and the Giesekus model. For the quadratic sPTT model, an equation for the inverse problem is also provided (being solved numerically). The effects of the Weissenberg number and mobility (Giesekus) parameters on the fluid flow are discussed, and the influence of the applied external electric field on the velocity and stress fields is studied.

For the sPTT models (linear, quadratic, and exponential), the dimensionless flow rate increases with εWi_κ^2 on account of the stronger shear thinning, with the exponential model showing higher velocities along the channel. The shear stress is null at the center of the channel and has a positive or negative slope depending on whether the pressure gradient is adverse ($\Gamma > 0$) or favorable ($\Gamma < 0$), respectively. In the channel core, the shear stress variation is linear as is typical of pressure gradient driven flow, but as the wall is approached the shear stress deviates from its linear variation due to the strong nonlinear variation of the electric potential in that region. Regarding the dimensionless elastic normal stress, $\bar{\tau}_{xx}$, the sharp near wall velocity gradient leads to a very large increase of the normal stress. The normal stress behavior near the walls is dramatically different from the bulk of the flow because in one case the EO forcing acts in the same direction as the pressure gradient forcing, hence the normal stress rises monotonically towards the wall whereas when the EO forcing acts in the opposite direction to the pressure forcing the normal stress exhibits a non-monotonic behavior.

For the Giesekus model, the dimensionless velocity increases with the mobility parameter, α, and the normal stress ,$\bar{\tau}_{xx}$, behaves qualitatively as for the sPTT model.

The normal stress $\bar{\tau}_{yy}$ is negative, meaning that there is compression in the y direction. Near the wall this compression increases, leading to an increase of the fluid stretch in the x direction (positive $\bar{\tau}_{xx}$), as shown before. Globally, we can conclude that when the electro-osmosis increases, the magnitude of both normal stresses, $\bar{\tau}_{xx}$ and $\bar{\tau}_{yy}$, tends to decrease at the center of the channel and increase near the walls, due to the sharp gradients at the EDL.

ACKNOWLEDGMENTS

J. M. Nóbrega and L. L. Ferrás acknowledge funding by FEDER through the COMPETE 2020 Programme and the National Funds through FCT—Portuguese Foundation for Science and Technology under Project No. UID/CTM/50025/2013. L. L. Ferrás would also like to thank funding by FCT through Scholarship No. SFRH/BPD/100353/2014. A. M. Afonso, F. T. Pinho, J. M. Nóbrega, and L. L. Ferrás acknowledge the funding by the National Funds through FCT under Project No. PTDC/EMS-ENE/3362/2014. A. M. Afonso would also like to thank FCT for the financial support through Scholarship No. SFRH/BPD/75436/2010.

[1] H. Bruus, *Theoretical Microfluidics, Oxford Master Series in Condensed Matter Physics* (Oxford University Press, Oxford, UK, 2008).
[2] F. F. Reuss, "Sur un nouvel effet de l'électricité galvanique," Mém. Soc. Imp. Nat. Moscou **2**, 327-337 (1809).
[3] N. Phan-Thien and R. I. Tanner, "New constitutive equation derived from network theory," J. Non-Newtonian Fluid Mech. **2**, 353-365 (1977).

[4] N. Phan-Thien, "A non-linear network viscoelastic model," J. Rheol. **22**, 259-283 (1978).
[5] N. Phan-Thien, "Squeezing of a viscoelastic liquid from a wedge: An exact solution," J. Non-Newtonian Fluid Mech. **16**, 329-345 (1984).
[6] H. Giesekus, "A simple constitutive equation for polymer fluids based on the concept of deformation-dependent tensorial mobility," J. Non-Newtonian Fluid Mech. **11**, 69-109 (1982).
[7] R. G. Owens, "A new microstructure-based constitutive model for human blood," J. Non-Newtonian Fluid Mech. **140**(1-3), 57–70 (2006).
[8] M. Moyers-Gonzalez, R. G. Owens, and J. Fang, "A non-homogeneous constitutive model for human blood. Part 1. Model derivation and steady flow," J. Fluid Mech. **617**, 327–354 (2008).
[9] H. Fam, J. T. Bryant, and M. Kontopoulou, "Rheological properties of synovial fluids," Biorheology **44**(2), 59–74 (2007).
[10] D. Burgreen and F. R. Nakache, "Electrokinetic flow in ultrafine capillary slits," J. Phys. Chem. **68**, 1084–1091 (1964).
[11] C. L. Rice and R. Whitehead, "Electrokinetic flow in a narrow cylindrical capillary," J. Phys. Chem. **69**, 4017–4024 (1964).
[12] S. Arulanandam and D. Li, "Liquid transport in rectangular microchannels by electroosmotic pumping," Colloids Surf., A **161**, 29–102 (2000).
[13] P. Dutta and A. Beskok, "Analytical solution of combined electroosmotic/pressure driven flows in two-dimensional straight channels: Finite Debye layer effects," Anal. Chem. **73**, 1979–1986 (2001).
[14] S. Das and S. Chakraborty, "Analytical solutions for velocity, temperature and concentration distribution in electroosmotic microchannel flows of a non-Newtonian bio-fluid," Anal. Chim. Acta **559**, 15–24 (2006).
[15] C. L. A. Berli and M. L. Olivares, "Electrokinetic flow of non-Newtonian fluids in microchannels," J. Colloid Interface Sci. **320**, 582–589 (2008).
[16] C. Zhao and C. Yang, "An exact solution for electro-osmosis of non-Newtonian fluids in microchannels," J. Non-Newtonian Fluid Mech. **166**, 1076-1079 (2012).
[17] C. Zhao and C. Yang, "Electro-osmotic mobility of non-Newtonian fluids," Biomicrofluidics **5**, 014110 (2011).
[18] A. M. Afonso, M. A. Alves, and F. T. Pinho, "Analytical solution of mixed electro-osmotic/pressure driven viscoelastic fluids in microchannels," J. Non-Newtonian Fluid Mech. **159**, 50-63 (2009).
[19] A. M. Afonso, M. A. Alves, and F. T. Pinho, "Electro-osmotic flows of viscoelastic fluids in microchannels under asymmetric zeta potential," J. Eng. Math. **71**, 15-30 (2011).
[20] H. M. Park and W. M. Lee, "Helmholtz–Smoluchowski velocity for viscoelastic electroosmotic flows," J. Colloid Interface Sci. **317**, 631–636 (2008).
[21] J. J. Sousa, A. M. Afonso, F. T. Pinho, and M. A. Alves, "Effect of the skimming layer on electro-osmotic–Poiseuille flows of viscoelastic fluids," Microfluid. Nanofluid. **10**, 107-122 (2011).
[22] S. Dhinakaran, A. M. Afonso, M. A. Alves, and F. T. Pinho, "Steady viscoelastic fluid flow between parallel plates under electro-osmotic forces: Phan-Thien–Tanner model," J. Colloid Interface Sci. **344**, 513-520 (2010).
[23] A. M. Afonso, F. T. Pinho, and M. A. Alves, "Electro-osmosis of viscoelastic fluids and prediction of electro-elastic flow instabilities in a cross slot using a finite-volume method," J. Non-Newtonian Fluid Mech. **179-180**, 55-68 (2012).
[24] R. B. Bird, P. J. Dotson, and N. L. Johnson, "Polymer solution rheology based on a finitely extensible bead-spring chain model," J. Non-Newtonian Fluid Mech. **7**, 213-235 (1980).
[25] T. Hayat, S. Afzal, and A. Hendi, "Exact solution of electro-osmotic flow in generalized Burgers fluid," Appl. Math. Mech. **32**, 1119-1126 (2011).
[26] A. M. Afonso, M. A. Alves, and F. T. Pinho, "Analytical solution of two-fluid electro-osmotic flows of viscoelastic fluids," J. Colloid Interface Sci. **395**, 277-286 (2013).
[27] M. W. Johnson, Jr. and D. Segalman, "A model for viscoelastic fluid behavior which allows non-affine deformation," J. Non-Newtonian Fluid Mech. **2**, 255-270 (1977).
[28] D. V. Boger and K. Walters, "Experimental dilemmas in non-Newtonian fluid mechanics and their theoretical resolution," Korea-Aust. Rheol. J. **12**(1), 27–38 (2000).
[29] M. D. Chilcott and J. M. Rallison, "Creeping flow of dilute polymer solutions past cylinders and spheres," J. Non-Newtonian Fluid Mech. **29**, 381–432 (1988).
[30] P. J. Oliveira and F. T. Pinho, "Analytical solution for fully developed channel and pipe flow of Phan-Thien–Tanner fluids," J. Fluid Mech. **387**, 271–280 (1999).
[31] M. A. Alves, F. T. Pinho, and P. J. Oliveira, "Study of steady pipe and channel flows of a single-mode Phan-Thien–Tanner fluid," J. Non-Newtonian Fluid Mech. **101**, 55-76 (2001).
[32] I. J. Rao and K. R. Rajagopal, "Some simple flows of a Johnson-Segalman fluid," Acta Mech. **132**, 209-219 (1999).
[33] J. Y. Yoo and H. C. Choi, "On the steady simple shear flows of the one-mode Giesekus fluid," Rheol. Acta **28**, 13–24 (1989).
[34] L. L. Ferrás, J. M. Nóbrega, and F. T. Pinho, "Analytical solutions for channel flows of Phan-Thien–Tanner and Giesekus fluids under slip," J. Non-Newtonian Fluid Mech. **171-172**, 97-105 (2012).
[35] P. Debye and E. Hückel, "Zur Theorie der Elektrolyte. I. Gefrierpunktserniedrigung und verwandte Erscheinungen [The theory of electrolytes. I. Lowering of freezing point and related phenomena]," Phys. Z. **24**, 185–206 (1923).
[36] A. Conlisk, "On the Debye-Hückel approximation in electroosmotic flow in micro- and nano-channels," AIAA Paper 2003-2869, 2003.